C. R. Physique 3 (2002) 1335–1359

Physique appliquée/*Applied physics*

DOSSIER

MÉCANISMES PHYSIQUES DU NUAGE D'ORAGE ET DE L'ÉCLAIR
THE PHYSICS OF THUNDERCLOUD AND LIGHTNING DISCHARGE

Fundamental processes in long air gap discharges

I. Gallimberti [a], G. Bacchiega [a], Anne Bondiou-Clergerie [b], Philippe Lalande [b]

[a] IRS srl, via Vigonovese 81, 35127 Padova, Italy

[b] ONERA, 29, av. de la division Leclerc, 92332 Châtillon, France

Note presented by Guy Laval.

Abstract The development of atmospheric lightning is initiated and sustained by the formation in virgin air of 'streamer corona' and 'leader' discharges, very similar to those observed in laboratory long sparks. Therefore, the experimental and theoretical investigations of these laboratory discharges have become of large interest to improve the physical knowledge of the lightning process and to develop self-consistent models that could be applied to new protection concepts.

In the present paper the fundamental processes of the subsequent phases of long air gap discharges are analyzed, from the first corona inception and development to the leader channel formation and propagation. For all these processes simulations models are discussed that have been essentially derived and simplified by the authors, in order to develop sequential time-dependent simulation of the laboratory breakdown, with both positive and negative voltages. The possibility of extending these models to the case of natural lightning is discussed in the companion paper, presented in this same volume. ***To cite this article: I. Gallimberti et al., C. R. Physique 3 (2002) 1335–1359.***

© 2002 Académie des sciences/Éditions scientifiques et médicales Elsevier SAS

streamer / leader / lightning / simulation / model / corona / discharge

Mécanismes physiques des décharges électriques sur de grands intervalles d'air

Résumé La formation d'un éclair débute par le développement, dans l'air vierge, de décharges électriques de type « corona » et « leader », semblables à celles observées en laboratoire haute tension sur de grands intervalles d'air. Ainsi, les études expérimentale et théorique des décharges de laboratoire sont un moyen pour comprendre les mécanismes physiques mis en jeu dans le développement de l'éclair. Ces études ont abouti au développement de modèles physiques qui permettent de simuler les décharges électriques et qui peuvent être utilisées pour optimiser les protections contre la foudre.

Dans cet article, les mécanismes physiques associés à chaque étape du développement d'une décharge électrique sont décrits. On analyse la formation du « corona » et la propagation du « leader ». Pour chacun des mécanismes, des modèles de simulation sont présentés et analysés. A partir de ces modèles élémentaires, les auteurs développent des modèles complets pour simuler la propagation spatiale et temporelle des décharges électriques positive et négative de laboratoire. L'adaptation de ces modèles au cas de l'éclair est discutée dans le papier associé dans ce même volume. ***Pour citer cet article : I. Gallimberti et al., C. R. Physique 3 (2002) 1335–1359.***

© 2002 Académie des sciences/Éditions scientifiques et médicales Elsevier SAS

décharge / modélisation / arc / leader / simulation / corona / éclair

E-mail address: bacchiega@irsweb.it (G. Bacchiega).

© 2002 Académie des sciences/Éditions scientifiques et médicales Elsevier SAS. Tous droits réservés
S1631-0705(02)01414-7/REV

1. Introduction

In recent years lightning initiation and development has been extensively investigated, both experimentally [1–3] and theoretically [4,5]. Particular interest has been devoted to lightning self-consistent models, which have been made possible by the improved knowledge of the physical mechanisms leading to the formation of electrical discharges [6–8], and by the increase of the capabilities of the computational resources.

It is well known that the electric field conditions, in which an electrical discharge can develop and propagate in air gap, change by orders of magnitude with the gap length: in small gaps (millimeter range) the electric field needed for breakdown is around 3×10^6 V·m^{-1}; in larger gaps (up to one meter) it becomes five time lower, around 5×10^5 V·m^{-1}, while it decreases to 1×10^5 V·m^{-1} for a ten meters gap. In the case of lightning discharges it has been shown [9] that the average field for stable propagation can be as low as 10^2 V·m^{-1}.

The aim of this paper is to describe the basic physical mechanisms, which control the subsequent phases of the discharge development and define the mean electric field needed for breakdown of increasing distances. In Section 2 a phenomenological description of the discharge development is given, for point-to-plane long gaps, under positive and negative applied voltages.

In Section 3 the subsequent phases (first corona inception and development, stem formation, leader head propagation, leader channel evolution) are analyzed in detail. The specific characteristics of the negative polarity pre-breakdown phenomena (space stem, pilot system, space leader) are discussed in Section 3.6. For each phase simplified simulation models are proposed, that have been derived by the authors in order to develop complete self-consistent models of air gap breakdown.

These complete models are finally presented for both positive and negative polarity in Section 4: they make possible the calculation of, as function of space and time, all the relevant discharge parameters (positions, advancement velocities, current, charge, luminous emission, etc.); the input data are simply the electrode geometry and the voltage waveshapes.

This paper is implicitly associated to the companion paper presented in this same volume [9], where the extension of these physical models to the lightning case will be described in details.

2. Discharge phenomena

2.1. Positive discharge

A typical development of a positive discharge in a point to plane gap submitted to a positive impulse voltage is shown in Fig. 1 [10]. The discharge is initiated by the formation of the first corona at time t_1. The corona consists of a number of narrow branched channels (‘streamers’), which develop from a common root. The mean electric field along the streamers filaments is about 5×10^5 V·m^{-1}, while their temperature is close to the ambient value. After one or more coronas, if the electrode potential is high enough, the leader channel inception itself takes place at time t_2, starting from the common root of the coronas (‘stem’). The leader appears as a weakly luminous channel which propagates almost continuously, unless the rate of increase of the voltage is too low: in this case, sudden re-illuminations associated with channel elongation appear during the propagation (‘restrikes’).

At the tip of the leader channel, the ‘leader corona’ is a diffused corona region which supplies the current necessary to sustain the leader propagation. Conversely, the advancement of the conductive channel into the gap keeps the electric field at the leader corona front sufficiently high to sustain the ionization processes. In the stable propagation conditions, the leader is associated with a low continuous current below 1 A and the internal electric field in the channel stays in the range of 1×10^5 V·m^{-1}. The coupled propagation of the leader and the leader corona continues until the corona streamers reach the plane: the subsequent final jump and arc phase that complete the breakdown process (time t_3).

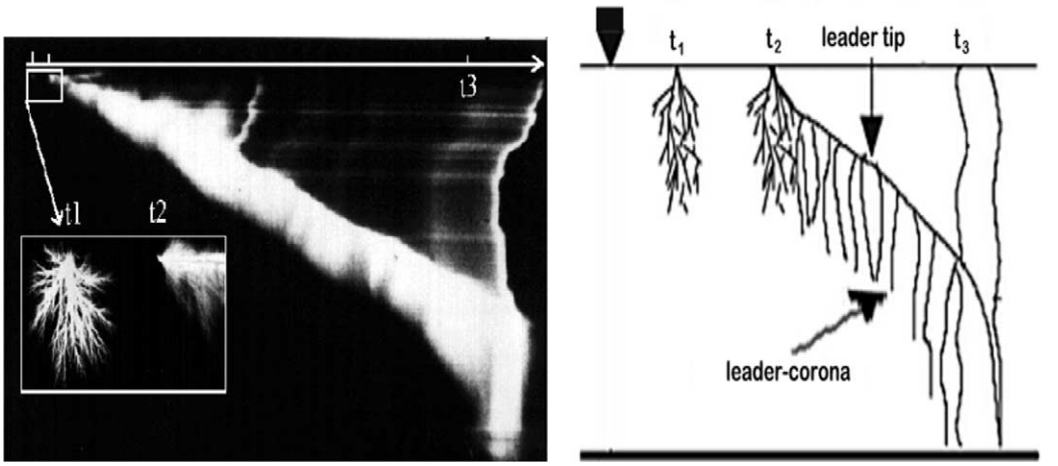

Figure 1. Streak photograph and sketch showing the development of a laboratory positive discharge (10 meter gap, $t_m = 500$ µs, $V_{max} = 2.5$ MV).

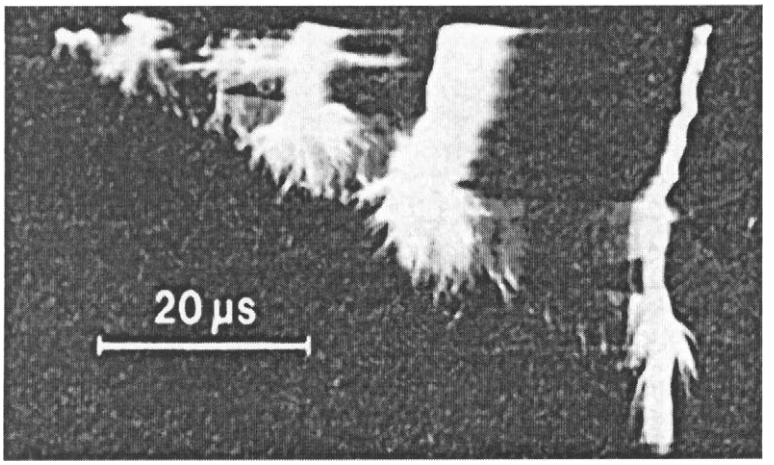

Figure 2. Streak photograph showing the development of a laboratory negative discharge (Gap length = 7 m, $V_{max} = 2.8$ MV; waveform 6/3000 µs).

2.2. Negative discharge

In a point to plane gap submitted to a negative impulse voltage (Fig. 2), the discharge is a non-continuous phenomenon which progresses through regular and discrete 'steps' separated by time periods of about 10 to 20 µs. Between two consecutive steps, complex phenomena can be observed with fast streak cameragrams [11]. This 'interstep' process can be divided into the phases shown in Fig. 3:

- the first negative corona (NC) develops at the H.V. electrode at time t_i; its branched filamentary structure appears similar to the first corona in positive polarity;
- after the first corona extinction, a short dark period takes place before the inception and development of a discharge process called 'pilot' (time t_1). A pilot system is made of two coronas of opposite polarity, the positive one (PC) develops upwards to the H.V. electrode while the negative one (NC) propagates downwards to the plane. At regular intervals new similar pilots develop from the tip of the preceding ones;
- at time t_2 a 'space leader' (SL) develops from a 'space stem', actually a previous pilot inception point. The space leader propagates as a bi-directional discharge, whose positive end propagates towards the

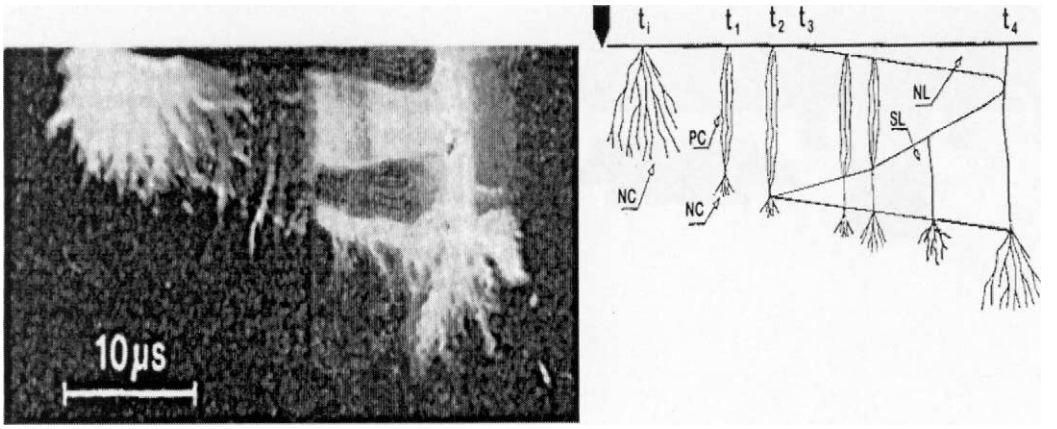

Figure 3. Streak photograph showing the interstep phase of a negative discharge (Gap length = 7 m, $V_{max} = 2.8$ MV; waveform 6/3000 μs).

cathode while the negative end progresses towards the anode. At time t_3 a negative leader (NL) starts from the negative electrode;

- at time t_4 the 'junction' of the space leader with the negative leader produces a strong illumination of the whole channel, while a new corona starts at its tips: this completes the step process. The entire phenomenon resumes and it is repeated until the discharge reaches the grounded plane.

2.3. Positive and negative discharge structure

According to the gap length and the voltage time rise the entire gap may be crossed in a few steps, whose size is generally between 1 and 2 m. It should be emphasized that the discharge process in both polarities may be regarded as similar: in both cases it consists in a coupled propagation of the leader channel with a feeding discharge at its head. In positive polarity, the feeding discharge is simply a corona discharge, while in negative polarity it is a complex structure including pilot systems and space leaders (Fig. 4). With positive polarity, the corona streamers propagate continuously because the electrons produced at their head drift in the direction of increasing field: therefore, they are not fully attached on electronegative molecules and are able to flow into the leader tip and sustain its propagation. In negative polarity, the electrons produced at the streamer front drift in the direction of decreasing field and attach at close distance to the corona: negative coronas are not able to inject a continuous current in the negative leader tip and the discharge evolves through more complex bi-directional processes.

3. Basic mechanisms

3.1. First corona inception

In air at atmospheric pressure free electrons can be generated by cosmic radiation or natural radioactivity: these electrons are generally attached to oxygen molecules to form negative ions. When a positive voltage is applied to H.V. electrode the negative ions drift into the high field region and may produce new free electrons by collisional detachment. The corona inception occurs when one of these free electrons, accelerated by the electric field in the region where ionization probability is higher than attachment probability ('active region'), forms an electron avalanche; the discharge actually starts when this electron avalanche is able to start a self-sustained ionization front. In a positive discharge, the electron avalanche moving towards the electrode creates a net positive charge which increases the electric field near the avalanche; if the resulting electric field is high enough, new avalanches can develop. The discharge process then consists of a series of avalanches developing into a plasma channel (Fig. 5(a)).

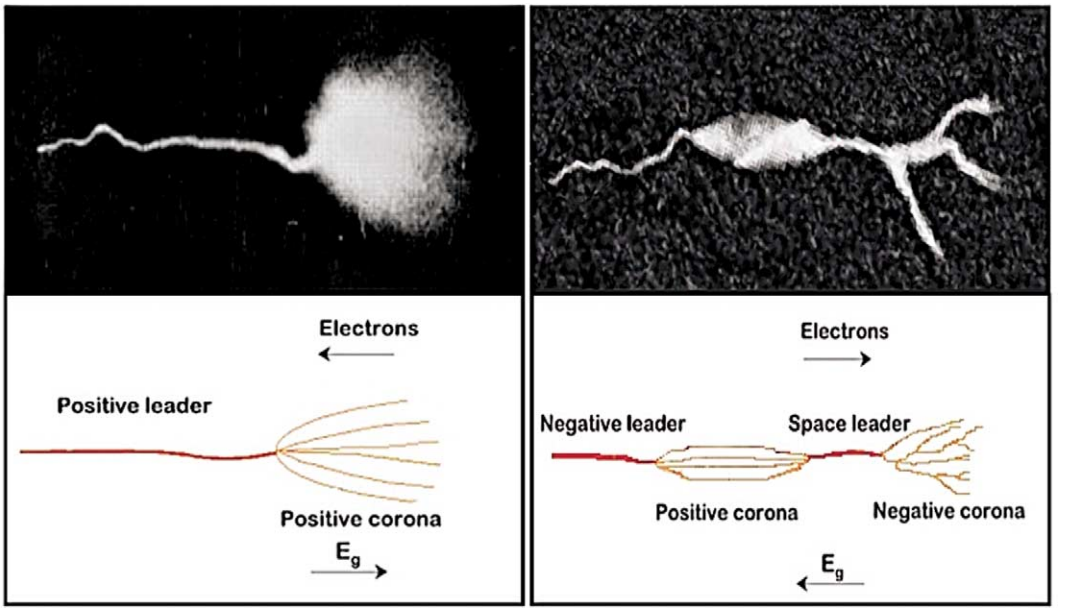

Figure 4. Positive and negative discharge structures with indication of the electron drift direction.

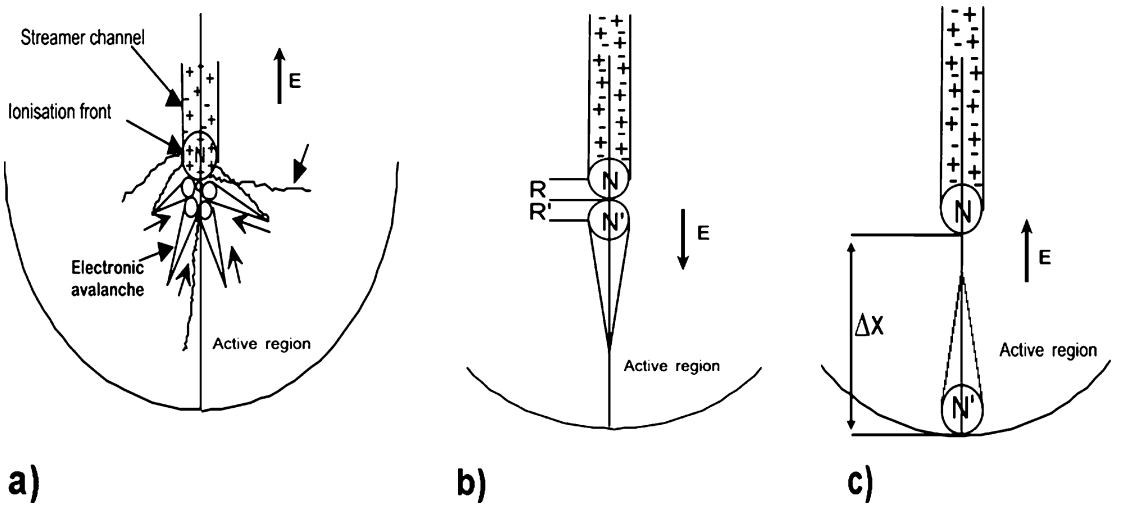

Figure 5. Schematic representation of positive streamer ionization front: (a) successive electron avalanches; (b) an equivalent electronic avalanche; (c) the equivalent avalanche in the case of negative streamers.

As a threshold for inception it can be assumed that the number of ions in the avalanche head must be higher than a minimum value N_{crit}.

The inception condition can therefore be described by the following equation [12–14]:

$$\exp\left[\int_{\Delta z} (\alpha - \eta)\, \mathrm{d}z\right] > N_{\text{crit}}, \tag{1}$$

where α and η are the ionization and attachment coefficients (dependent on the electric field), Δz is the length of the active region. The value of N_{crit} varies with applied field and is around 0.55×10^8.

The minimum inception field can be computed by empirical laws similar to the Peek's equation [15]

$$E = E_0 \delta M \left(1 + \frac{K}{\sqrt{\delta R_{\text{eq}}}}\right), \tag{2}$$

where

δ is the relative air density,

E_0 the breakdown field (3×10^6 V/m) in a uniform field gap at STP,

R_{eq} the equivalent curvature radius of the electrode, and K and M are predefined constants.

In the case of negative discharge the electron avalanches move in the opposite direction and the net charge is negative; however, the inception conditions defined for positive corona can be applied also to the negative corona. Consequently, it is possible to use the same equations for both polarities.

For almost uniform short gaps (in the millimeter or centimeter range) the breakdown is realized just after the corona inception; the average breakdown field has therefore a value which is not far from the minimum ionization field E_0 for which α becomes larger than η (in air at atmospheric pressure is about 3×10^6 V·m^{-1}).

3.2. Corona propagation

Experimental evidence, based mostly on short gap measurements has shown that the streamers which form the corona are made essentially of two regions: (i) the streamer head or active region where the luminous emission and ionization processes take place; (ii) the streamer channel or passive region where the electrons generated in the tip flow towards the H.V. electrode and remain attached to the electronegative molecules. The streamer head has the following characteristics [15]:

- it contains a net electrical charge;
- the rotational temperature do not exceed 330 K while the vibrational temperature is raised largely above 1000 K; the vibrational energy is then relaxed in long times because of the long lifetimes of the vibrational state;
- the electron energy at the streamer head is in the range 5–15 eV which corresponds to average fields of 10–15 MV·m^{-1} [16];
- the streamer head radius is in the range of 10–30 μm and its density is of the order of 10^{21} m^{-3}.

The streamer channel has the following characteristics:

- the channel radius, estimated in short gaps, is in the range of 10–30 μm and the corresponding electron density is around 5×10^{19}–10^{21} m^{-3} [17]. In long gaps, however, the electron density can be much lower, because the attachment process reduces the number of free electrons;
- the current is essentially an electronic conduction current flowing in a resistive regime along all the streamer channel: $I = \pi a^2 \sigma E$ (a is the filament radius, σ its conductivity, E local field);
- the three body and dissociative attachment have been demonstrated to be the dominant electron collision process.

Streamer simulation models are essentially based on the original streamer theory proposed by Raether [12] and Loeb and Meek [14]. The streamer head is assumed to be the front of a space charge wave, where positive ions and excited molecules are highly concentrated as the result of previous ionization and excitation phenomena (Fig. 5(a)). The decay of the excited states produces by photo-ionization a distribution of secondary electrons around the wave front, which in turn form new electron avalanches. The drift of the electron avalanches in to the positive charge causes its neutralization and the remaining positive ions lead to the advancement of the wave front into the gap.

The simulation of streamer formation and propagation is based on the solution of the continuity equations for electrons, positive and negative ions, including the effects of ionization, attachment, recombination,

electron diffusion, combined with the estimation of secondary electrons produced by photo-ionization, and coupled with the solution of the Poisson's equation.

A simplified model was proposed by Gallimberti [18]. In this model the series of avalanches at the head of the streamer are represented by a single equivalent avalanche producing the same overall space charge (Figs. 5(b) and 5(c)).

In these conditions it is possible to replace the continuity equations with an overall energy balance condition and calculate step by step the number of ions at the tip of the streamer, the net charge created, the velocity and the extent of the corona. The energy balance at the streamer front can be written in the form:

$$W_{\mathrm{g}} + \Delta W_{\mathrm{pot}} = W_{\mathrm{l}}, \tag{3}$$

where W_{g} is the energy gained by electrons in the equivalent avalanche (from the external circuit through the forces of the geometric field), W_{pot} is the variation of the potential energy including the geometric potential component (changes in the applied voltage distribution) and the self potential component (concentrations of positive ions in the streamer front) and W_{l} is energy lost by the electrons in collisions with gas molecules (ionization, dissociation, excitation, attachment, scattering, ...).

In divergent field configurations, it has been shown that the charge at the tip increases in the high field region, reaches a maximum and then drops until propagation stops. The maximum in this curve corresponds to the electric field value where the propagation would be energetically stable. In regions where the applied field is higher then the stability value, the energy gain is larger than the losses, and therefore the charge in the streamer front increases, while in regions of lower field values the propagation occurs at the expense of the potential energy of the charge in the tip region. In this case, the propagation stops when this potential energy is no longer sufficient for the production of new ionization.

A simplified version of this model was implemented by Badaloni et al. [19] and used in [6]. For positive and negative streamers the number of positive or negative ions, respectively, in the streamer head can be calculated as a function of the advancement coordinate along a field line (x):

$$N_+(x) = N_+(0) + \frac{2eR+\mu}{4a}\left[V(0) - \frac{\beta}{2eR+\mu}x - V(x)\right], \tag{4}$$

$$N_-(x) = N_-(0) + \frac{R(e\Delta x+\mu)}{2a\Delta x}\left[V(0) - \frac{\gamma}{e\Delta x+\mu}x - V(x)\right], \tag{5}$$

where $V(x)$ is the electrostatic potential, R the streamer head radius assumed constant, Δx the negative advancement step (Fig. 5(c)), μ the coefficient for energy gain, β and γ the coefficients for energy losses in positive and negative polarity respectively, and $a = 0.4e^2/(4\pi\varepsilon_0)$.

The values of the stability field in positive and negative polarity are expressed by the following equations:

$$E_{\mathrm{s}+} = \frac{\beta}{2eR+\mu} \approx 5.10^5\ \mathrm{V/m}, \tag{6}$$

$$E_{\mathrm{s}-} = \frac{\gamma}{e\Delta x+\mu} \approx 7.510^5\ \mathrm{V/m}. \tag{7}$$

These stability fields can be used within a simplified method to evaluate the corona extension using the electrostatic potential distribution before corona development. It has been shown that the stability field is equivalent to the average field along the streamer extension [20]; therefore, if the average field is fixed, the corona length is directly given by the geometric construction of Fig. 6.

Under reasonable simplifying assumptions, the total space charge Q can be determined from the dashed area in Fig. 6 and distributed in the corona volume.

$$Q = K4\pi\varepsilon_0 \int_0^{x_s} U_2(x) - U_1(x)\,\mathrm{d}x, \tag{8}$$

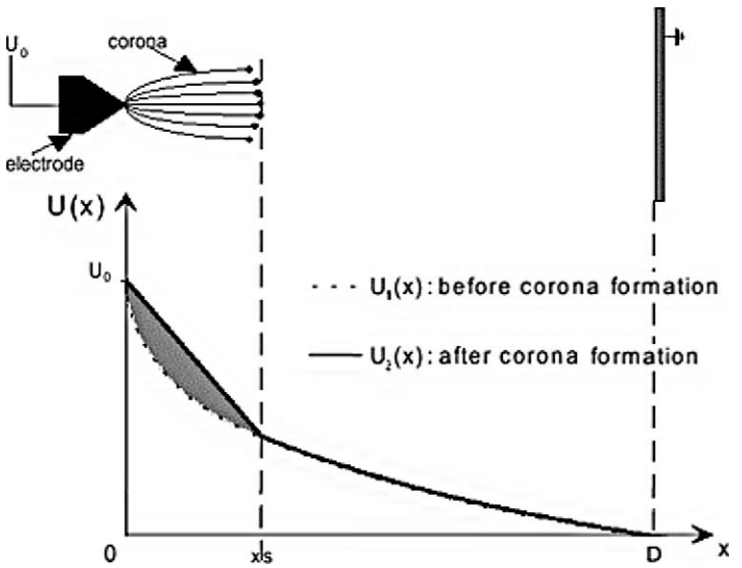

Figure 6. Potential distributions in the rod-plan gap before and after first corona formation.

where K is a geometric factor taking into account all the streamers characteristics (length and number of streamers in the corona, [21]). It is possible to estimate the magnitude of the current pulse from charge calculation by using a bi-exponential pulse with a short rise time of 10–50 ns and a decay time of 200–500 ns consistent with measurements.

For gap length ranging from a few centimeter up to 1 meter, the breakdown is realized when the streamer front is able to cross the entire gap ('direct breakdown'): in this case the average breakdown field is the streamer stability field $E_{s+}E_{s-}$ (Eqs. (6) and (7)) and is around $5–7.5 \times 10^5$ V·m^{-1}.

3.3. Leader channel formation

Electrical discharges in long air gaps continue their advancement after the occurrence of streamer corona through the development of a new channel structure called leader. The major difference between leader and streamer channels is the thermodynamic and hydrodynamic conditions.

In positive and negative polarity the transition from corona to leader channel first happens at the root of the branched structure of the corona discharge (stem).

Experimental evidence of temperature increase from corona to the leader has been measured by spectroscopic and strioscopic measurements [22,23]: the gas temperature rises from 300 K to 1000–1200 K. The current created by the streamers converge on the stem region and increases its thermal energy due to Joule effect. The energy input produces significant effects in the stem channel:

- a temperature increase of the gas molecule by Joule effect;
- an hydrodynamic expansion;
- a reduction of the gas density;
- a detachment of the negative ions due to the combined effects of the increase of gas temperature and reduced field E/n_h (where n_h is the density of neutrals).

These effects increase drastically the conductivity of the stem and the electric field at its tip. This makes possible the start of a second corona which drives the leader advancement. However, only part of the Joule energy EI, transferred by the electrons to gas molecules, in the stem contributes immediately to the temperature rise. The gas molecules store the internal energy in different forms: translational, rotational, vibrational and electronic excitation, dissociation and ionization. On the time scale of the corona to leader transition, only translational, rotational and electronic excitation can be assumed to be in local thermodynamic equilibrium (LTE) at the gas temperature in the stem, and to contribute directly to the

temperature increase. Chemical energy (dissociation and ionization) can be neglected while the vibrational energy is relaxed on a time scale comparable or longer than that of the leader channel formation. The complete relaxation process has been numerically simulated and an equivalent relaxation time constant has been estimated (see [18] for computation results) taking into account different kind of molecules, including small concentration particles as H_2O and CO_2 which have a resonant vibrational exchange with the N_2 molecule.

In order to model the leader formation, the stem is assumed to be composed by three kinds of particles: electrons, ions and neutral particles. For each species the conservation equations of mass, momentum and energy are to be considered, together with the field and current density equations.

The inception condition of the leader is attained if the gas temperature reaches a critical temperature T_{cr} (around 1500 K). Using a cylindrical homogeneous model of the stem, and with the hypothesis specified in [18], it is possible to compute the evolution of the temperature in the stem solving two balance equations for thermal enthalpy and vibrational energy of the gas molecules:

$$\begin{aligned}
&\frac{\mathrm{d}}{\mathrm{d}t}\left(\frac{7}{2}kT_{\mathrm{h}}n_{\mathrm{h}}\pi a^2\right) = (f_{\mathrm{e}} + f_{\mathrm{r}} + f_{\mathrm{t}})EI + \frac{\pi a^2(w_{\mathrm{v}}(T_{\mathrm{v}}) - w_{\mathrm{v}}(T_{\mathrm{h}}))}{\tau_{\mathrm{vt}}},\\
&\frac{\mathrm{d}}{\mathrm{d}t}\left(\pi a^2\varepsilon_{\mathrm{v}}\right) = f_{\mathrm{v}}EI - \frac{\pi a^2(w_{\mathrm{v}}(T_{\mathrm{v}}) - w_{\mathrm{v}}(T_{\mathrm{h}}))}{\tau_{\mathrm{vt}}},\\
&w_{\mathrm{v}}(T_{\mathrm{v}}) = n_{\mathrm{h}}\pi a^2\frac{\varepsilon_0}{\exp(\varepsilon_0/kT_{\mathrm{v}}) - 1},
\end{aligned} \tag{9}$$

where T_{h} and T_{v} are the translational and vibrational temperature of neutrals, a is the stem radius, f_{e}, f_{r}, f_{t} and f_{v} are the fractions of the Joule energy EI transferred to the molecules in the form of electronic, rotational, translational and vibrational excitation, w_{v} is the vibrational energy per unit volume and ε_0 the average vibration excitation step.

The initial conditions of the simulation of the stem $a = 35$ µm; $T_{\mathrm{h}} = 300$ K; the current I injected at the stem root is the corona current; the inception time is the time at which temperature T_{h} becomes larger then T_{cr}. Fig. 7 shows two stem simulation examples. For relatively large curvature radius (left) the first corona current is strong enough to raise neutral temperature T_{h} above critical temperature before the corona full development, so that allowing the leader inception only after some hundreds of nanoseconds. In the case of a small curvature radius (right) the leader inception intervenes only some microseconds after the first corona, as neutral temperature needs to wait for the relaxation of vibrational temperature in order to attain the critical inception value.

3.4. Leader channel advancement

A typical picture of a leader corona development is shown in Fig. 8, where the leader appears as a channel, which connects the high voltage electrode to the luminous conic structure of the corona. The leader head appears as a bright point moving forward on a tortuous path so that the axial component of the velocity has random fluctuations while the effective velocity sets to a more stable value almost proportional to the measured current:

$$v_{\mathrm{L}} = \frac{I_{\mathrm{L}}}{q_{\mathrm{L}}}. \tag{10}$$

The constant q_{L} physically represents the charge needed for a unit length advancement of the leader channel; it has been measured, depending on voltage waveform and absolute humidity, between 20 and 50 $\mu\mathrm{C}\cdot\mathrm{m}^{-1}$.

The basic mechanisms that governs the leader head advancement are the same as those leading to its first formation (as described in the previous section) with the major difference that the transition region (stem or leader head) is moving with a stable velocity v_{L} across the gap. The current and field lines are converging

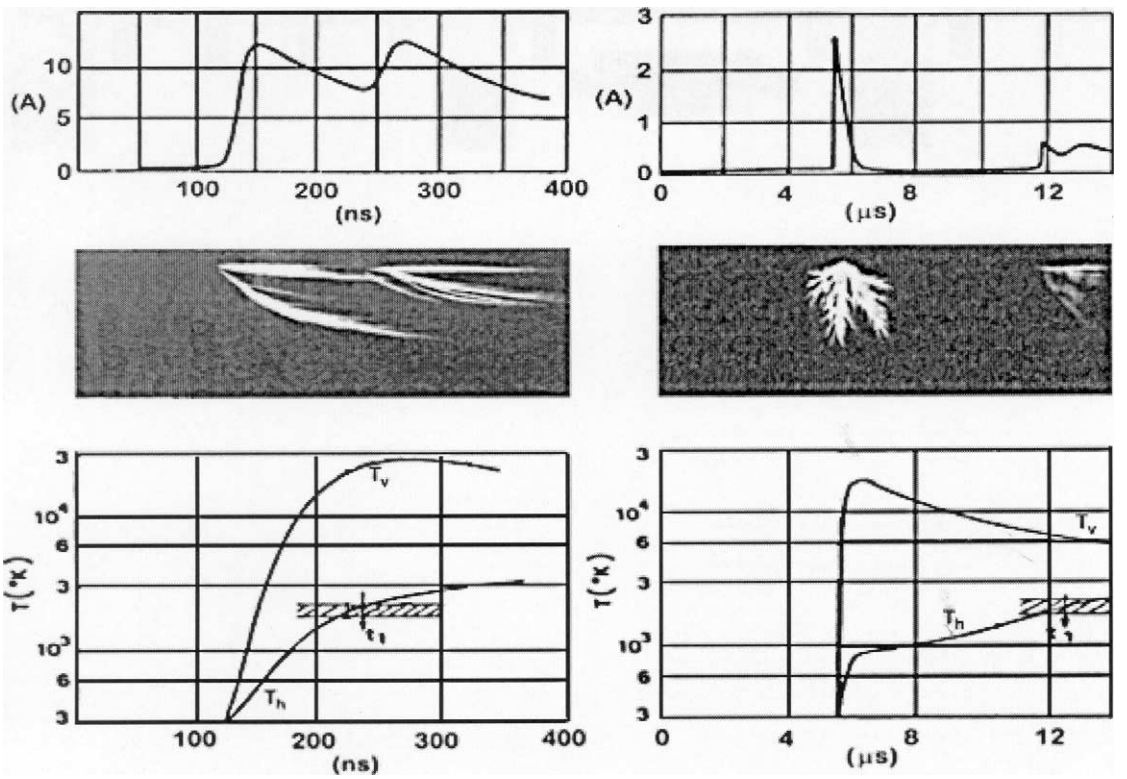

Figure 7. First and second corona current pulse, streak image and correspondent temperature simulations at the stem for large curvature radius (left) and small curvature radius (right).

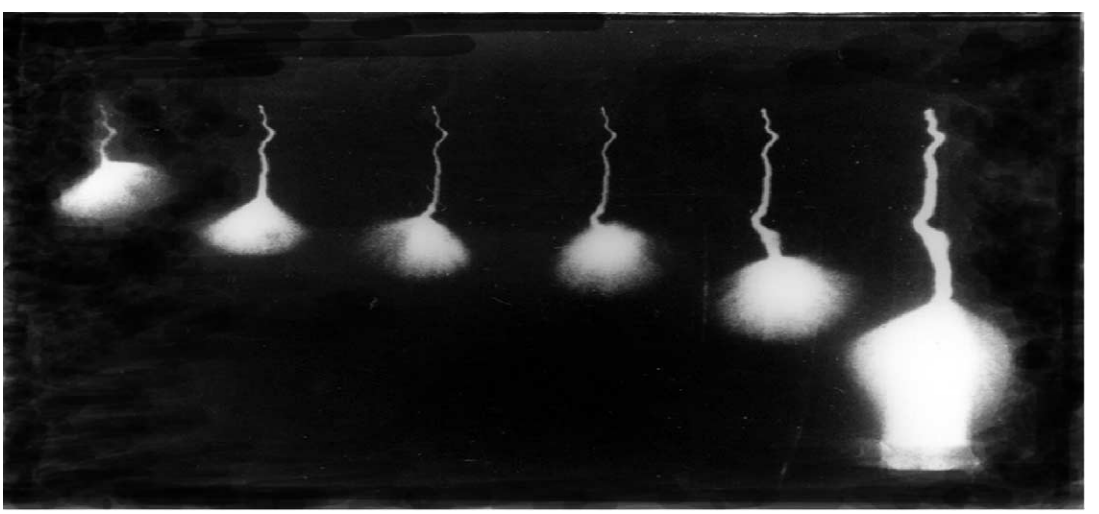

Figure 8. Frame photograph of leader channel connected to the luminous corona conic structure (10 meter cone-plane gap, 500/10000 μs wave).

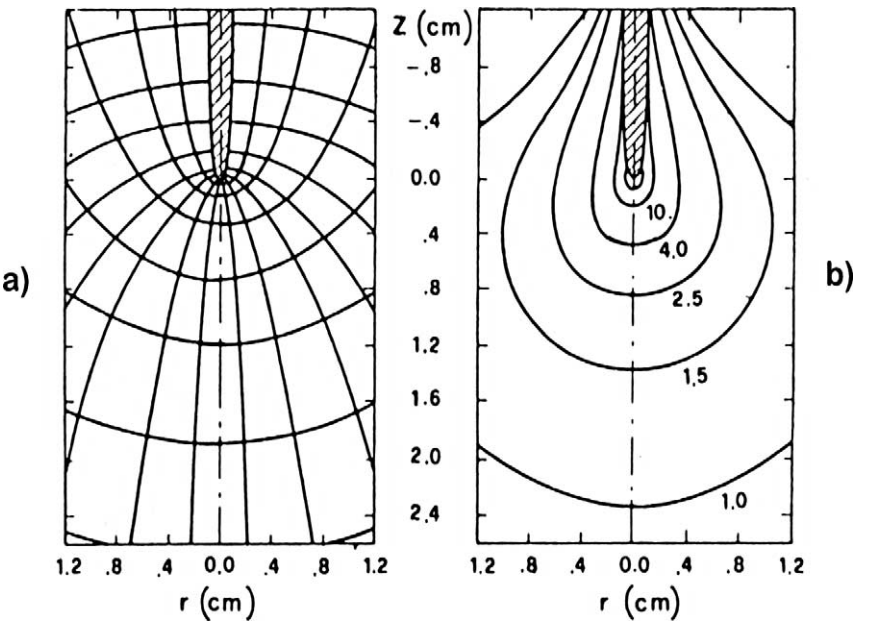

Figure 9. Schematic representation of the leader head transition region: (a) field and current lines; (b) line of constant power input.

towards the leader head (Fig. 9), leading to an exponential increase of the Joule power transferred to the gas molecules. Then the leader tip can be assimilated to the boundary of a punctual explosion translated with a velocity v_L, and the leader profile can be described as a paraboloid with a tip radius around 25 μm [24], which is consistent with experimental observations [25,26].

Introducing a reference frame of parabolic coordinates (φ, η) moving into the gap with constant velocity v_L, it is possible to write an energy conservation equations system similar to Eq. (9) and search for a steady-state solution, with the condition that, at the leader head surface, the temperature is raised from the ambient temperature T_0 to the critical value T_{cr} [13].

The following are obtained:

$$\begin{aligned} &\frac{7}{2}kn_h(T_{cr}-T_0) = (f_e+f_r+f_t)\int_{z_t}^{z_l} JE\frac{dz}{v_L} + w_v\left\langle\frac{\tau_l}{\tau_{vt}}\right\rangle, \\ &w_v = f_v\int_{z_t}^{z_l} JE\frac{dz}{v_L} - w_v\left\langle\frac{\tau_l}{\tau_{vt}}\right\rangle, \end{aligned} \tag{11}$$

where J is the current density, z_l and z_t are the coordinates of the boundary of leader and transition region, w_v represents the value of vibrational energy per unit volume at the leader surface, $\langle\tau_L/\tau_{vt}\rangle$ is the fraction of vibrational energy that is relaxed into thermal form in the transition region, τ_L is the leader transit time in the transition region which depends on the leader velocity.

This formulation allow the computation of leader velocity as:

$$v_L = \left[f_e+f_r+f_t+f_v\frac{\langle\tau_l/\tau_{vt}\rangle}{1+\langle\tau_l/\tau_{vt}\rangle}\right]\frac{2}{7kn_h\Delta T_L}\int_{z_t}^{z_l} JE\,dz \tag{12}$$

and the estimation of the charge per unit length q_L necessary for thermal transition (see Eq. (10)) as function of leader potential at tip U_{lt}:

$$q_L = K_g \frac{k n_h \Delta T_L}{U_{lt}(f_e + f_r + f_t + f_v\langle\tau_l/\tau_{vt}\rangle/(1+\langle\tau_l/\tau_{vt}\rangle))}, \tag{13}$$

where K_g is a geometrical constant defined by the transition region geometry.

As seen from the experimental results q_L is almost constant during the propagation, as the transition region remains self-similar and the leader tip potential almost constant. From Eq. (13), it is possible to see that the charge per unit leader length q_L essentially depends on the applied potential wave shape (affecting U_{lt}), on leader velocity (affecting the leader transit time τ_L) and on humidity (affecting the vibrational relation time τ_{vt}), in good agreement with experimental observations (Fig. 10).

The current I_L injected in the leader tip corresponds to that flowing across the transition region during stable propagation at velocity v_L; it can be calculated through the Shockley–Ramo theorem [6] taking into account the motion of both the positive charge in the streamer front, and the negative charge of the electrons drifting towards leader head. It results to be:

$$I_L = eN_1N_s(v_s - v_L)\frac{E_L(z_s)}{U_{lt}} + \frac{eN_1N_s}{\eta D_s}(v_e)\left[1-\exp(-\eta x)\right]\frac{\langle E_L\rangle}{U_{lt}}, \tag{14}$$

where

N_1 is the number of filaments in the corona head,
N_s is the number of ions in each streamer head,
v_s and v_L are respectively the corona and leader advancement velocities,
$E_L(z_s)$ is the electric field at the corona front,
D_s is the depth of the corona front,
η is the attachment coefficient for electrons,
v_e is the electron average velocity within the corona region,
U_{lt} is the leader tip potential.

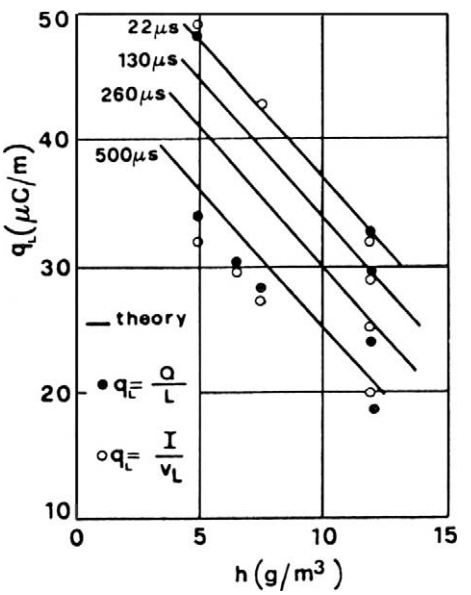

Figure 10. Comparison between computed and experimental values of charge per unit length q_L for different wavefront durations and humidities.

The number of ions N_s can be estimated [6] from an energy balance similar to Eq. (3):

$$\frac{dN_s}{dt} = \frac{N_s v_s}{U_s}\left[E_{s+} - \frac{\beta - \mu E_{s+}}{2eR_s}\right] \tag{15}$$

with U_s being the potential at the corona front.

The velocity of the corona front v_s depends linearly upon N_s and the geometric field E_g at that point, and so it can be deduced from the following differential equation [13]:

$$\frac{dv_s}{dt} = \alpha_1(k_1 + k_2 v_s)(E_g - E_{s+}) + \alpha_2 \frac{dE_g}{dt}, \tag{16}$$

where α_1, α_2, k_1 and k_2 are constants derived by numerical simulations.

3.5. Leader channel characteristics

The leader channel appears as a luminous thin channel, connecting the corona region to the H.V. electrode, whose cross-section is expanding in time. The channel diameter depends essentially on the total charge flown through the leader section. The luminous diameter is between 0.5 and 1 mm for a 1.5 m gap and between 2 and 4 mm for 10 m gap. The thermal diameter measured by Schlieren techniques [27] in 1.5 meter gap increases from 0.2 mm, to 0.5–0.6 mm in case of withstand and 0.8–0.9 mm before breakdown.

From charge and field measurements the average field along the leader channel has been estimated [28, 29]: it decreases with leader length from 5×10^5 V·m^{-1} to 10^5 V·m^{-1}. The ratio of light to current is practically constant for all visible wavelength: this indicates that excitation occurs essentially by electronic collision under constant reduced field E/n_h. As the leader gradient E is decreasing with time, the constant value of E/n_h is consistent with a leader expansion that decreases the gas density n_h.

Mathematical models of the leader channel are very complex because they should account for thermodynamic and hydrodynamic processes coupled with the electrical characteristics of the plasma channel. In the model proposed by Braginskii [24], the leader channel is represented as a homogeneous core of radius a, surrounded by a thin dense shell. The pressure, temperature and particle densities are assumed to be constant over the core section, the variations of these parameters to the values of the undisturbed gas being concentrated in the shell. The model is based on a simplified solution of the mass, momentum and energy conservation equations for electrons, positive ions and neutrals. In the original Braginskii model, the expansion can be simulated as an expansion of a cylindrical piston with no exchange of energy between the channel and the surrounding air. However, the radiated and conducted heat is absorbed in the shock-wave shell: this energy is transferred to the surrounded air which is heated from ambient temperature to the temperature of the neutrals in the channel. The expanding channel is in this case described as a 'porous piston'.

3.5.1. *Mass conservation equations*

As radial derivatives disappear across the core section, the mass conservation equations for a unit length channel becomes:

$$\begin{aligned} \frac{dN_e}{dt} &= \frac{dN_+}{dt} = \dot{N}_e, \\ \frac{dN_h}{dt} &= -\dot{N}_e + \dot{N}_d + \dot{N}_h^{por}, \end{aligned} \tag{17}$$

where N_e, N_+ and N_h are the number of electrons, positive ions and neutral molecules per unit length, $\dot{N}_d$ and $\dot{N}_e$ are the net rates of dissociation and ionization respectively, N_h^{por} is the rate of externally added

neutrals which is given by:

$$\left(C_V T_h + p_c \frac{\pi a^2}{N_h}\right) \frac{dN_h^{por}}{dt} = Q_R + Q_T. \tag{18}$$

The radiative losses Q_R consist of retardation and recombination; the losses due to thermal conduction $Q_T = Q_{Te} + Q_{Th} + Q_{T+}$ are the sum of contributions by electrons, neutrals and positive ions respectively (complete expressions can be found in [24]).

In order to determine the electron production rate $\dot{N}_e$ to be used in (17), two main reactions and their inverse reactions have to be considered:

– ionization by electron impact and electron–ion recombination

$$e + A \underset{K_{pa}}{\overset{K_{ap}}{\rightleftarrows}} 2e + A^+; \tag{19}$$

– three body recombination and ionization by molecule impact

$$e + A^+ \underset{S_{pa}}{\overset{S_{ap}}{\rightleftarrows}} A + B; \tag{20}$$

where K_{ap} and S_{ap} are the reaction rates and K_{pa} and S_{pa} are the rates for the inverse reactions.

The evolution of the density of electrons can thus be written as:

$$\frac{dn_e}{dt} = n_e n_h K_{ap} - n_e^2 n_+ K_{pa} + n_h^2 S_{ap} - n_e n_h n_+ S_{pa}. \tag{21}$$

Using the assumption that the reactions and their inverse reactions are in equilibrium, the relationship between the reaction rates can be given by Saha's equation:

$$\frac{K_{ap}}{K_{pa}} = \beta_{T_e} = \frac{2g_+}{g_a} \frac{2\pi n_e k_B T_e}{h} \exp\left(\frac{\varepsilon_e}{k_B T_e}\right), \tag{22}$$

$$\frac{S_{ap}}{S_{pa}} = \beta_{T_h} = \frac{2g_+}{g_a} \frac{2\pi n_e k_B T_h}{h} \exp\left(\frac{\varepsilon_e}{k_B T_h}\right), \tag{23}$$

where g_+ and g_a are the multiplicity of the ground states of ions and molecules, ε_e the ionisation energy and h is Planck's constant.

Introducing $\beta = n_e^2/n_h$, the linear density of electrons can be then calculated as:

$$\frac{dN_e}{dt} = \dot{N}_e = N_e \nu_i \left(1 - \frac{\beta}{\beta_{T_e}}\right) - N_e N_p \frac{\eta}{\pi a^2} \left(1 - \frac{\beta_{T_h}}{\beta}\right), \tag{24}$$

where $K_{ap} = \nu_i n_h$ and $S_{pa} = \eta n_h$, ν_i is the ionisation rate and η is the recombination rate.

Under stationary condition, the ionisation degree in the leader channel can be calculated from Eq. (24) as a function of T_e and T_h (Fig. 11). At relatively low temperature (T_h below 5000 K) the ionisation is essentially due to electron collision, and it depends on electron temperature T_e; at high gas temperature T_h the ionisation is essentially due to thermal collisions between molecules and it depends only on T_h (thermalized leader).

3.5.2. *Momentum conservation equations*

The momentum conservation equations for all the particles can be combined together, so that the collision terms vanish [30]. Under the assumption of plasma neutrality within the core, and of identical average

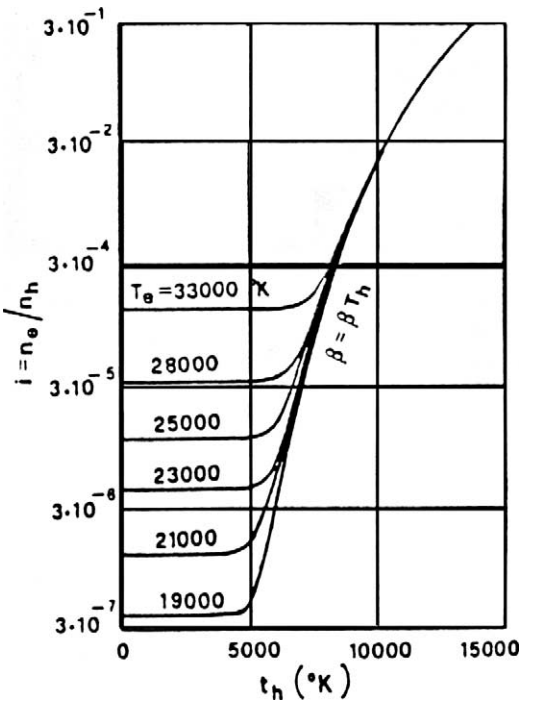

Figure 11. Ionization degree in the leader channel, depending on both the electron temperature T_e and the gas temperature T_h.

expansion velocities for all particles $\langle \dot{a} \rangle$, the resultant equation is:

$$\frac{\mathrm{d}[(N_e m_e + N_+ m_+ + N_h m_h)\langle \dot{a} \rangle]}{\mathrm{d}t} = 2\pi a \left[\langle p_c \rangle - \langle p_s \rangle \right], \tag{25}$$

where $\langle p_c \rangle$ and $\langle p_s \rangle$ represent the average values of the pressure in the core and shell respectively.

The pressure p_c in the channel core is given by the sum of all partial pressures:

$$\pi a^2 p_c = N_e k_B T_e + N_p k_B T_p + N_h k_B T_h. \tag{26}$$

The pressure p_s in the shock-wave shell is assumed to be given by the following expression:

$$p_c = \left(1 + \frac{2\gamma}{1+\gamma} (M^2 - 1) \right) p_0, \tag{27}$$

where p_0 is the ambient pressure and γ the quotient between the thermal capacities at isobaric and isovolumetric transformations. M is the Mach number and is given by

$$M = \frac{\gamma + 1}{4} \frac{\langle \dot{a} \rangle}{c} \left(1 + \sqrt{\left(\frac{4}{\gamma + 1} \frac{c}{\langle \dot{a} \rangle} \right)^2 + 1} \right), \tag{28}$$

where c is the speed of sound in the ambient air.

3.5.3. *Energy conservation equations*

If the ionic component of the total current I is neglected [31], the energy conservation equations become:

$$\frac{\mathrm{d}}{\mathrm{d}t}\left[N_{\mathrm{e}}\left(\frac{3}{2}k_{\mathrm{B}}T_{\mathrm{e}}+\varepsilon_{\mathrm{e}}\right)\right]+p_{\mathrm{e}}\frac{\mathrm{d}(\pi a^2)}{\mathrm{d}t}=EI-\dot{C}_{\mathrm{eh}}-\dot{C}_{\mathrm{e}+}-Q_{\mathrm{R}}-Q_{T_{\mathrm{e}}}, \tag{29}$$

$$\frac{\mathrm{d}}{\mathrm{d}t}\left[N_{+}\frac{5}{2}k_{\mathrm{B}}T_{+}\right]+p_{+}\frac{\mathrm{d}(\pi a^2)}{\mathrm{d}t}=\dot{C}_{\mathrm{e}+}-\dot{C}_{+\mathrm{h}}-Q_{\mathrm{T}+}, \tag{30}$$

$$\frac{\mathrm{d}}{\mathrm{d}t}[N_{\mathrm{h}}C_{\mathrm{V}}T_{\mathrm{h}}]+p_{\mathrm{h}}\frac{\mathrm{d}(\pi a^2)}{\mathrm{d}t}=\dot{C}_{\mathrm{eh}}+\dot{C}_{\mathrm{ph}}-Q_{T_{\mathrm{h}}}, \tag{31}$$

where p_{e}, p_{+} and p_{h} are the electrons, ions and neutrals partial pressures, $\dot{C}_{\mathrm{e}+}$, $\dot{C}_{\mathrm{eh}}$, $\dot{C}_{+\mathrm{h}}$ are the rate of energy exchange between the different kinds of particles (the corresponding expressions being given in [18], EI is the Joule source term and electrons and positive ions, which is mainly governed by Coulomb collisions:

$$\dot{C}_{\mathrm{ep}}=N_{\mathrm{e}}\frac{3m_{\mathrm{e}}}{m_{\mathrm{p}}}\nu_{\mathrm{ep}}k_{\mathrm{B}}(T_{\mathrm{e}}-T_{\mathrm{p}}), \tag{32}$$

where ν_{ep} is the frequency of Coulomb collisions.

If the leader channel is assumed to behave as a resistive conductor, the Poisson equation may be replaced by a simple ohmic relation:

$$E=\frac{I}{e\mu_{\mathrm{e}}N_{\mathrm{e}}}, \tag{33}$$

where μ_{e} is the electron mobility which should account at high ionization degree also for electron–ion collisions

$$\mu_{\mathrm{e}}=\frac{e}{m_{\mathrm{e}}(\nu_{\mathrm{eh}}+\nu_{\mathrm{e}+})}. \tag{34}$$

3.5.4. *Calculated results*

The set of Eqs. (17)–(34) can be solved to calculate the temporal evolution of the leader channel parameters. The initial conditions represent the state of a leader section just behind the head, where all the negative ions have been detached. The following initial parameters can be used: $T_{\mathrm{h}}=15\,00$ K; $T_{\mathrm{e}}=15000$ K; $p_{\mathrm{c}}=101.3$ kPa; $a=1$ mm.

In Fig. 12 the evolution of the channel characteristics is presented for a weak current case (0.3 A continuous current with a few ampere impulse superimposed), which may correspond to most of the laboratory cases: the gas temperature is slowly increasing and saturates around 3500–4000 K, while the electron temperature remains around 25 000 K: the thermodynamic conditions are far away from LTE. The electric field is slowly decreasing with the increase of the temperature from 3×10^5 to 1×10^5, indicating an almost constant value of E/n_{h}. The current pulse induces a dynamic response in electron temperature and electric field which is rapidly dumped to the stationary value.

In Fig. 13 the evolution of the channel characteristics is presented for a strong current case (a series of 90 A pulses), which may correspond to a strong negative discharge in a laboratory gap or to the lightning case: after the first pulse the gas temperature is rapidly increasing above 6000 K, while the electron temperature is falling rapidly around the same value, approaching the LTE conditions. The electric field falls at the same time to 10^2 V·m^{-1}. The subsequent current pulses produce rapid transients of the electric field and electron temperature which are rapidly damped to the previous LTE values.

The presented results show that, when the temperature is below 5000 K, the leader channel is far from LTE and the ionization is due essentially to electron–molecules collisions. In the case of higher temperatures the leader reaches LTE ('thermalized leader') and the ionization is essentially due to molecular collisions.

In laboratory long gaps, up to 10 m, the breakdown is realized when the streamer-leader system is able to cross the entire gap. Under usual conditions the discharge current does not exceed a few amperes, and therefore the leader channel does not have a sufficient energy input to become thermalized: the average

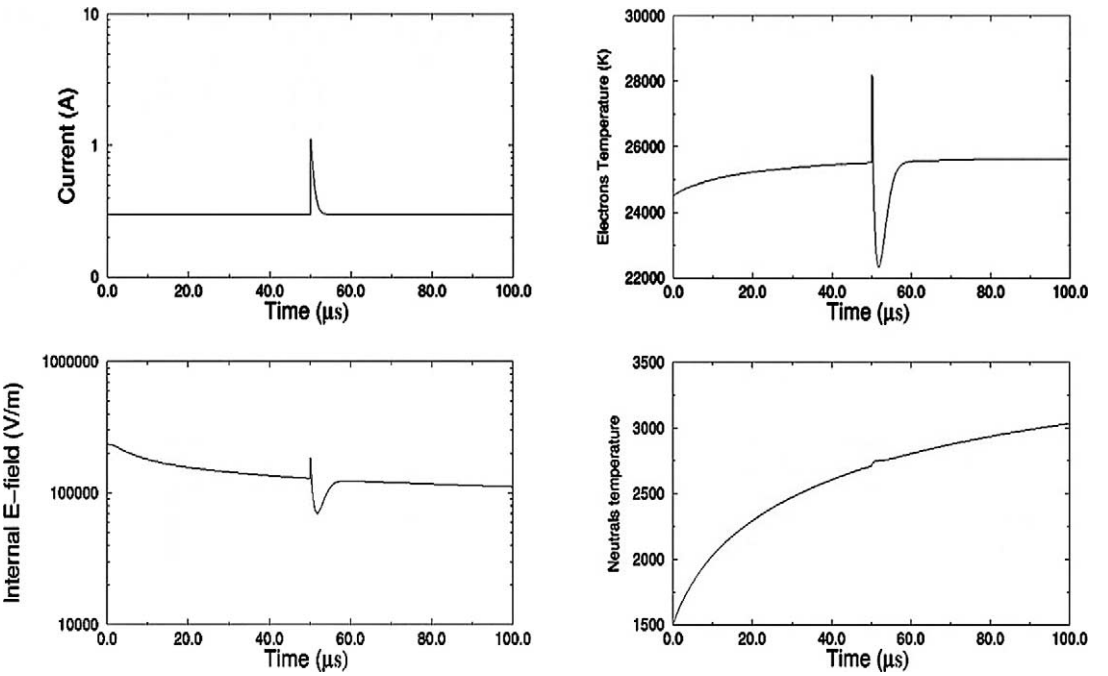

Figure 12. Model input 3 A impulse current and computed internal leader resistance as function of time (left). Electronic and neutral temperature as function of time (right).

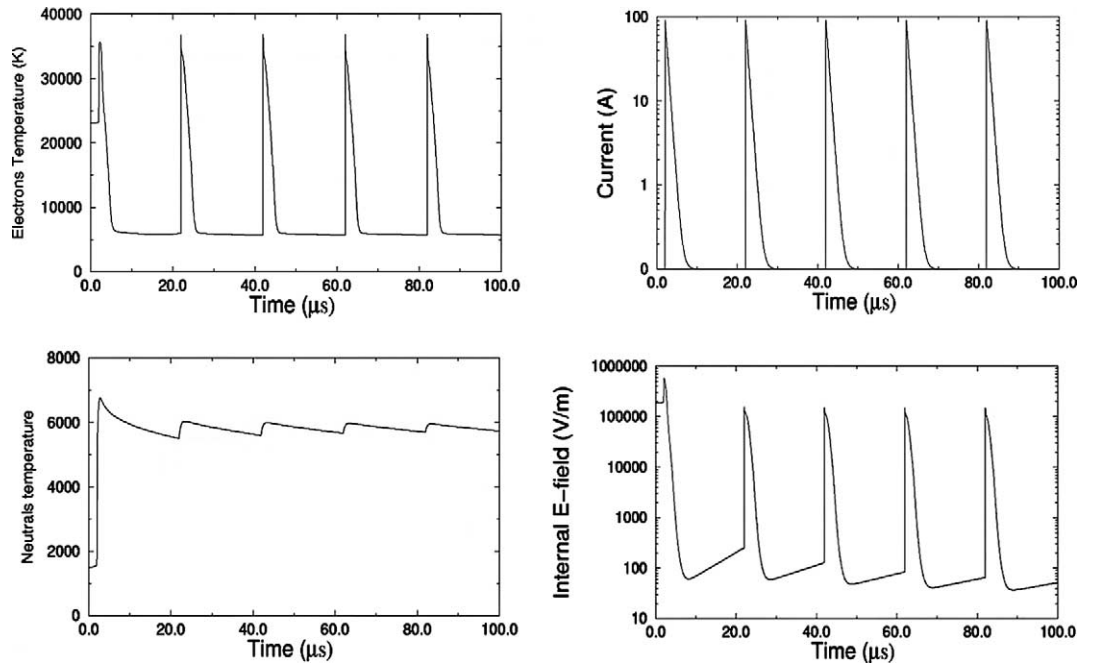

Figure 13. Model input 90 A impulse current and computed internal leader resistance as function of time (left). Electronic and neutral temperature as function of time (right).

breakdown field is therefore in the range 3 to 1×10^5 V·m^{-1}. In longer gaps, particularly under negative polarity, and in the case of natural lightning, the current can raise to much higher values: the leader channel can therefore become thermalized, and the average breakdown field can decrease to a few 10^2 V·m^{-1}.

3.6. Specific processes in negative polarity

3.6.1. *Pilot systems*

As seen in Section 2.2, the negative discharge advancement involves the formation of successive pilot systems starting after the first corona extinction near the boundary of the streamer front.

A thoroughly and satisfactory explanation of physical processes occurring at the pilot system is still not available. However a consistent approach has been presented in [7]. As streamer filaments are plasma channels of limited conductivity, after the extinction this plasma undergoes a classical relaxation process which tends to increase the local potential towards the H.V. electrode potential, in order to reduce to zero the internal field. The relaxation time constant depends essentially on the corona's nonuniform geometry and charge distribution. A nonuniform multiple resistor-capacitance line model has been retained to describe this relaxation phenomenon. Resistance values are defined upon local conductivity conditions derived from the corona model (see Eqs. (4) and (5)), which provides the number of ions per unit length. The linear capacitance has been considered constant. The relaxation process increases the potential at the streamer front and may create the electric field needed for the inception of a new forward negative corona and a backward positive corona. If the inception conditions are established the development of the two opposite coronas can be computed over the relaxed potential using the approximation of constant field within the steamers channel detailed in Section 3.2.

The evolution of the potential profile during the pilot inception process is given in Fig. 14:

(a) initial distribution of the geometric potential;

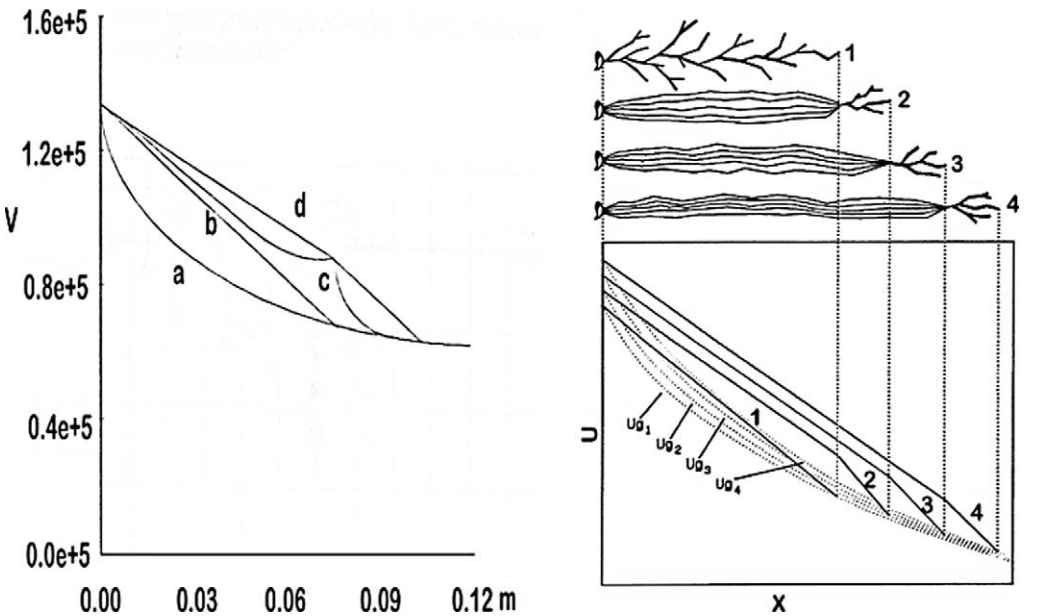

Figure 14. Left: evolution of the potential profile before (a) and after (b) negative corona development, during the relaxation process (c) and after the pilot formation (d). Right: evolution of the potential distribution during a sequence of 3 successive pilots.

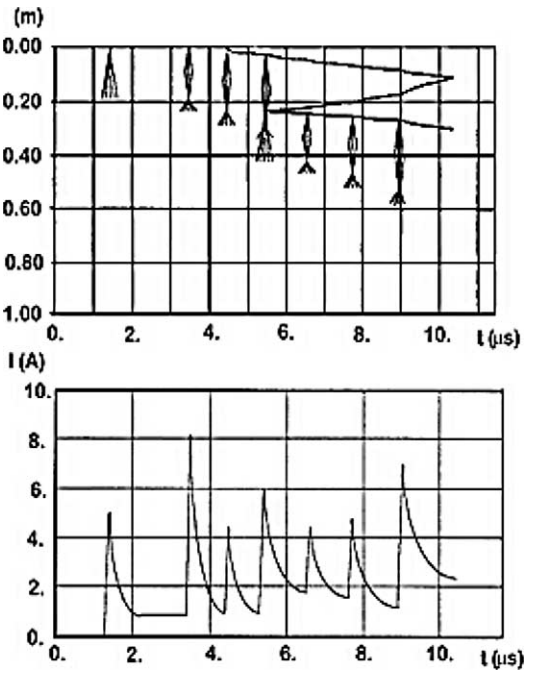

Figure 15. Simulation of pilot systems and space leader in a 2 m point to plane gap.

(b) potential distribution after the formation of a negative corona represented as a constant field region equal to the stability field E_{s-} (see Eqs. (6) and (7));
(c) evolution of the potential distribution during the relaxation process (calculation with a classical RC line equation);
(d) if inception conditions are locally reached at the pilot tip, formation of two coronas of opposite polarities (represented as constant fields regions). The corresponding charge injected in the channel can be calculated using Eq. (8).

After corona extinction, a new relaxation process can be simulated using the RLC line approach with a modified resistance (the channel conductivity can be evaluated from the ionic densities using Eqs. (4) and (5)). Subsequent pilot formation can therefore be described in sequence using this method (see the scheme of Fig. 14 right).

If the applied voltage is not sufficient, the relaxation process does not lead to the conditions for inception of a new pilot and an arrest condition of the whole discharge propagation is the obtained.

The calculation of the charge associated with each new pilot system can be deduced from the difference of the potential profiles at times (c) and (d) using Eq. (8). An example of the simulation of a sequence of pilot systems is given: it appears that the characteristic times, velocities and pilot charges are in good agreement with experimental results. The current in Fig. 15 has an impulsive component associated with the bipolar coronas and a continuous component due to the relaxation process in the RC line. The current is calculated using a predefined bi-exponential shape.

3.6.2. *Space leaders*

Streak cameragrams show that, under certain conditions, a pilot system can evolve towards a ‘space stem’, from which a leader can be initiated. This leader, called ‘space leader’, is a bi-directional discharge. Two conditions must be fulfilled for inception of the space leader:

(1) the temperature at the space stem is raised up to a critical temperature where the detachment of negative ions strongly increase the conductivity;

(2) the electric field at the edge of the stem is high enough to start new streamers which will feed the bi-directional leaders development.

As in the case of the transition of a stem into a leader (see Section 3.3), the energy balance given by Eq. (9) can be used in order to calculate the temperature evolution of the space stem and check if condition (1) is satisfied. The calculation of inception conditions of new steamers requires us to choose an equivalent electrostatic representation of the space stem: from streak and frame images, it can reasonably be assumed that it is equivalent to an ellipsoid of about 10 mm length. Its edge curvature radius evolves with time due to thermal expansion; it can be calculated using the model of channel expansion described in Section 3.5.

After space leader inception, its advancement is governed by the current produced within the pilot systems that drives the whole discharge advancement. The advancement can be simulated, using Eq. (10) to estimate the velocity of the positive and negative ends of the space leader:

$$v_{L+} = \frac{I}{q_{L+}}, \qquad v_{L-} = \frac{I}{q_{L-}}. \tag{35}$$

The values of the charge per unit length necessary for the space leader bi-directional advancement have been evaluated from experimental measurements [8]: $q_{L^+} = 73.5$ μC and $q_{L^-} = 145$ μC.

3.6.3. *Junction of space leader and negative leader*

As described in Section 2.2, a negative leader is also initiated from the cathode and propagates towards the space leader positive end until the two discharges undergo a junction process leading to a strong re-illumination of the whole channel associated with a large current pulse, and resulting in the formation of a longer negative leader. The charge flowing through the discharge at the time of the junction can be calculated from Eq. (8). The potential distribution immediately before the junction is given by the solution of the RC line simulation (Fig. 16(a)). The potential distribution after the junction of the 2 leaders (Fig. 16(b)) is evaluated using the following hypothesis:

– the internal field in the new negative leader can be neglected due to the thermalization process intervening after strong current pulses (as described in Section 3.5);
– at the tip of the new negative leader, the sudden rise of space leader potential causes the inception of a negative corona; its final length can be determined using the geometric construction described in Fig. 6.

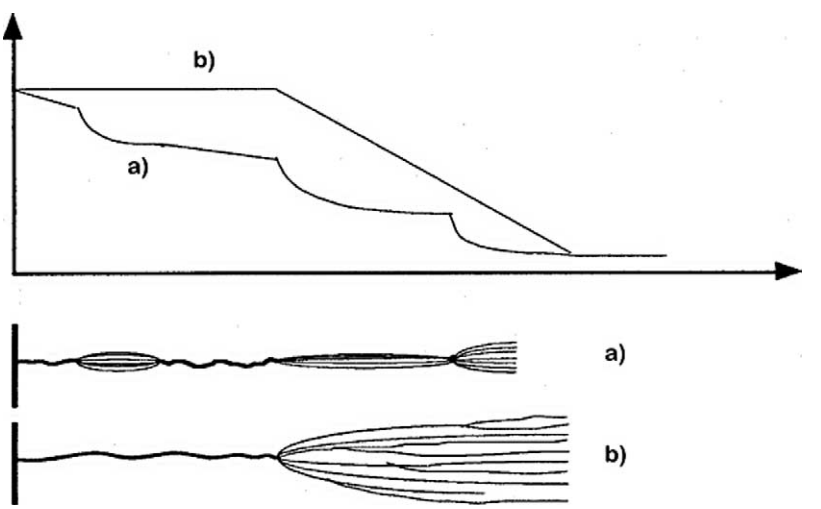

Figure 16. Distribution of potential (a) before and (b) after the junction between the space leader and the negative leader.

4. Numerical simulations of the breakdown

4.1. Electric field calculation

The first step for a numerical simulation of the breakdown processes is the calculation at every time and point in the gas of the electric field, which is the driving force of the discharge development. The electric field calculations in the models described in the present paper may be analytical or numerical.

Analytical solutions are based on an equivalent representation of the streamer-leader system (Fig. 17). The discharge is represented as a rotational symmetric configuration, in an ellipsoidal-hyperboloidal coordinate system, in which the focal point is on the rod center. The rod and leader channel are represented by semi-infinite hyperboloids and the corona space charge region by an ellipsoid. The analytical calculation results from the sum of three components: the electric field due to electrodes and the leader channel, the field due to corona space charge, and the field due to the image of the space charge into the electrodes and the leader [6].

More accurate solutions has been obtained using numerical methods derived from the classical Charge Simulation Method [32].

4.2. Positive discharges

A complete model for the simulation of all phases of a positive discharge has been proposed by Bondiou and Gallimberti [6]. This model is time dependent and simulates in sequence the inception of the first corona (Section 3.1, Eq. (1) or (2)), the development of the first and second coronas (Section 3.2, Eqs. (4)–(8)); it then calculates the inception time of the leader channel (Section 3.3, Eq. (9)). Once the leader channel is formed, the simulation of the propagation of its head is based on the solution of the equation system (10), (13)–(15) and (16), while the internal conditions of the leader channel along its length are calculated by use of Eqs. (17)–(34). At each time step, the new position of the leader and corona heads, the space charge value and the potential of the leader tip are calculated; the electric field distribution along the propagation axis can therefore be evaluated using analytical approximations.

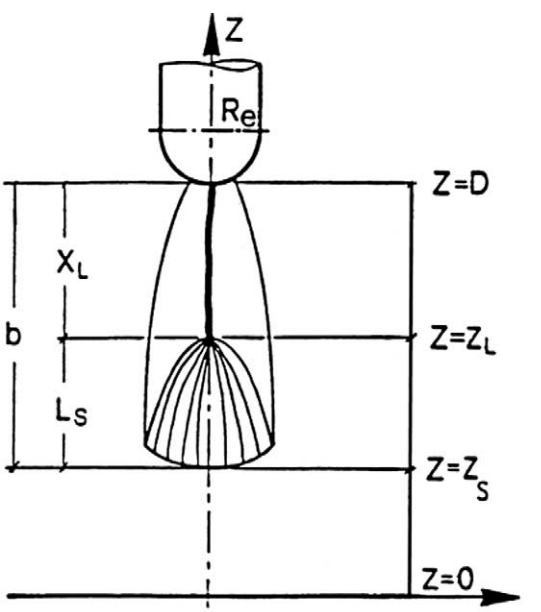

Figure 17. Representation of the discharge for analytical calculations of the field and potential distributions.

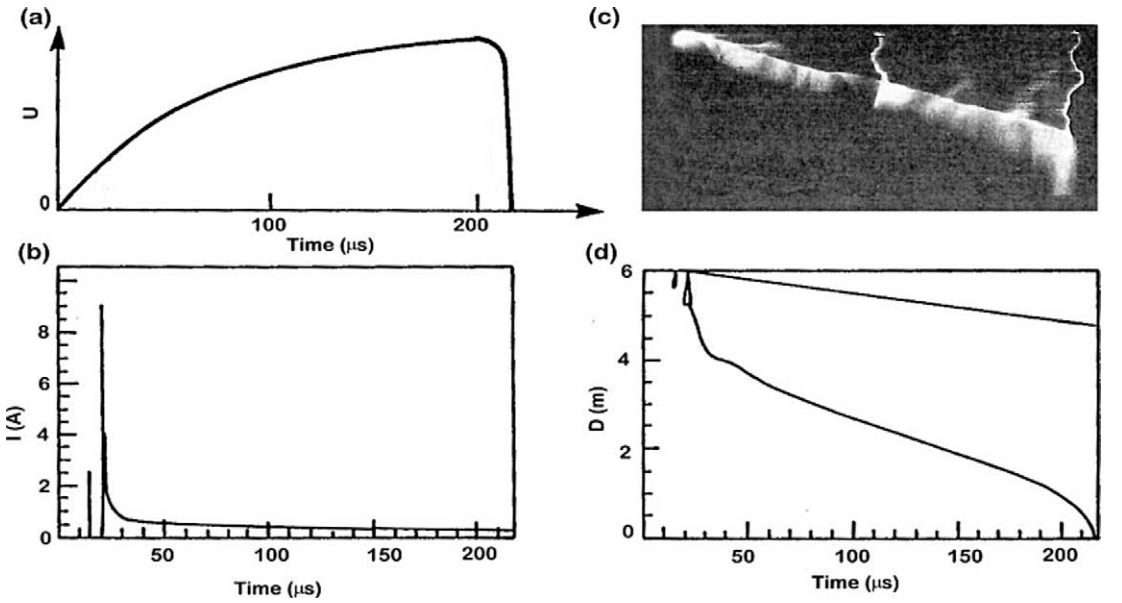

Figure 18. (a) Applied voltage ($V_{max} = 1550$ kV); (b) Computed current for the applied voltage; (c) Discharge development streak photograph in a point-plane 7 meter gap; (d) simulation of corona and leader tip advancement.

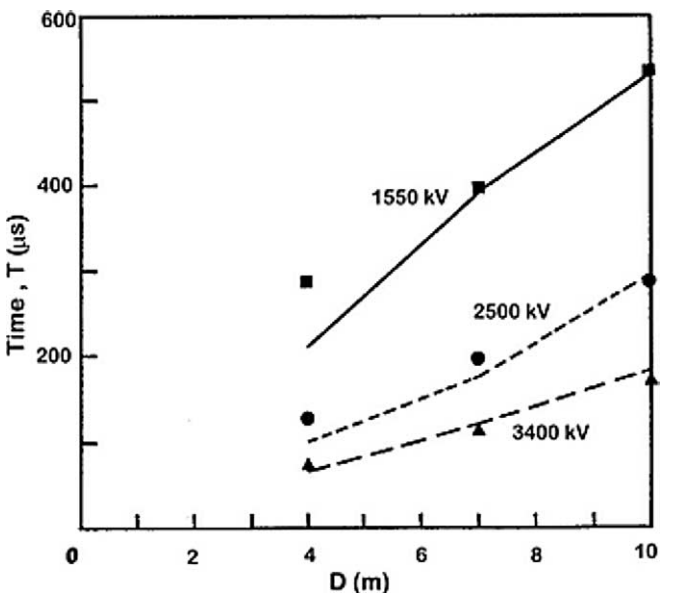

Figure 19. Computed time to breakdown (continuous and dotted lines) as function of gap length and applied voltage. Experimental values (●, ■, ▲) are given for comparison.

An example of simulation of the positive discharge development across a 6 meter rod-plane gap is given in Fig. 18. The model has been tested in various configurations and its results have been successfully compared to experimental results [6].

The model makes possible to predict the minimum breakdown voltages for different gap lengths and voltage waveshapes, and the breakdown times for different applied overvoltages (Fig. 19); furthermore it has shown to have a good stability and a good dynamic response with respect to external perturbations of the propagation conditions [6].

4.3. Negative discharge

A similar self-consistent time-dependent model has been derived also for negative discharges; the major difference is that the propagation of the corona in front of the leader head (Eqs. (15) and (16)) has been replaced by the more complex representation of the pilot-system, the space stem and the space leader.

The model simulates the different phases of the stepped propagation in long gaps and has been validated in different rod-plane configuration studied by the Renardières Group [11].

Figs. 20 and 21 show typical simulation results.

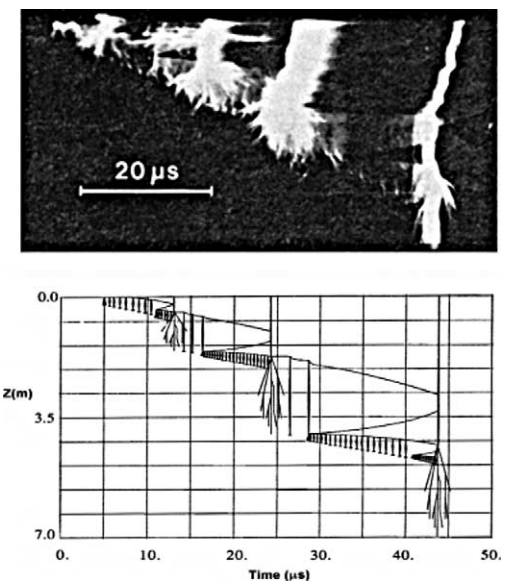

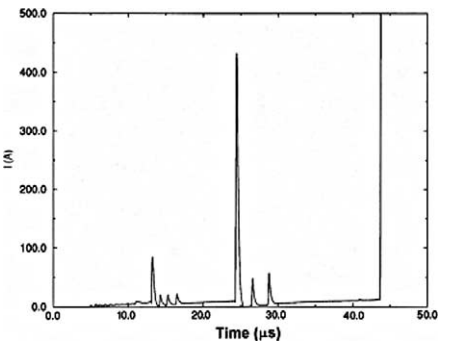

Figure 20. Streak photograph, streak simulation and computed current of a negative discharge in a point plane configuration (Gap = 7 m, $V_{max} = 2.8$ MV; waveform 60/3000 µs).

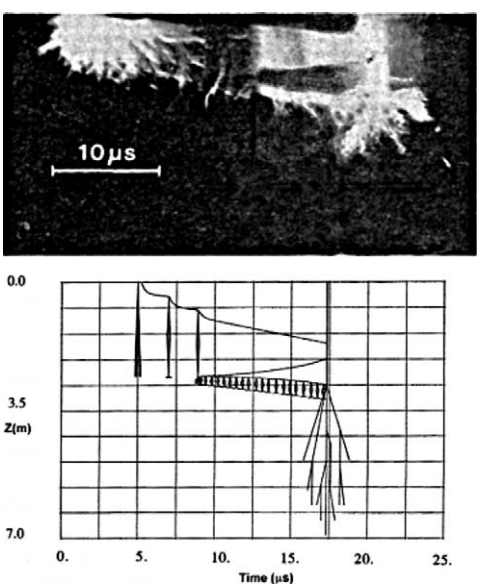

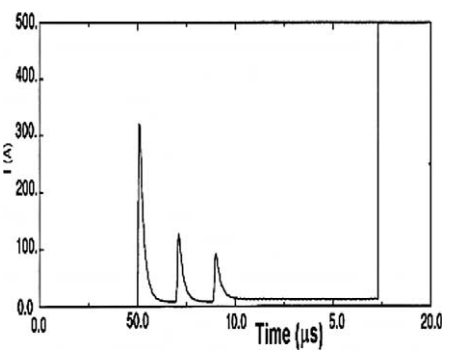

Figure 21. Streak photograph, streak simulation and computed current of a negative discharge in a point plane configuration (Gap = 7 m, $V_{max} = 2.8$ MV; onde 6/3000 µs).

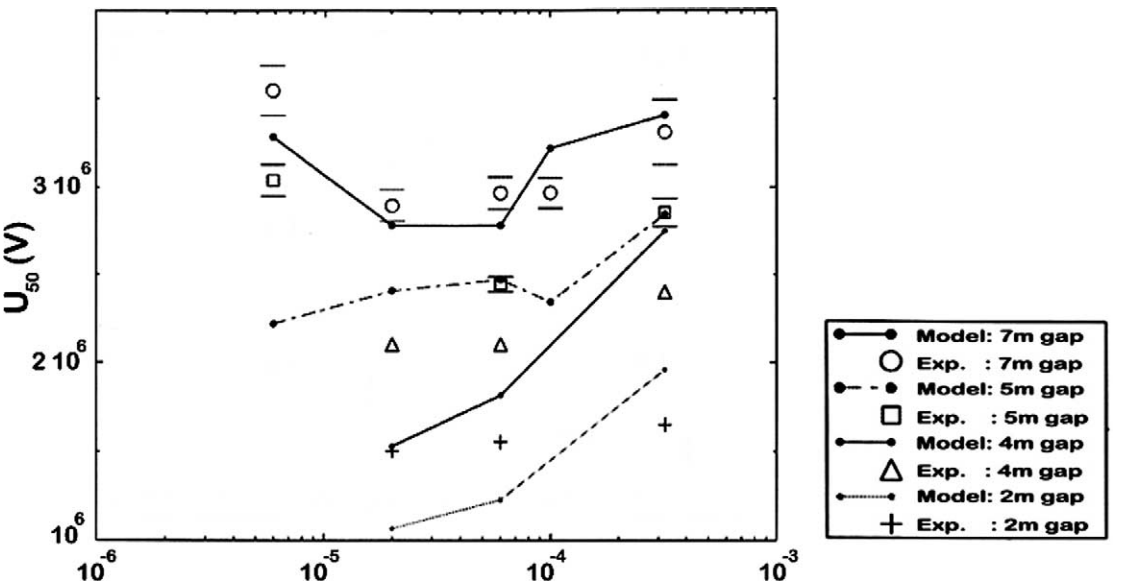

Figure 22. Experimental and model computation of U_{50} Breakdown voltage as a function of time to crest voltage T_{cr} for different rod-plane gap.

The overall computed space-time characteristics of the discharge are in good agreement with experimental measurements. The average stepping period results between 15 and 20 μs. The calculated current is composed by a series of pulses which are consistent with current measurements [33].

The model has been positively tested for different voltage amplitudes and waveforms as well as for different gap lengths. As for the positive polarity the model makes possible to predict minimum breakdown voltages and times, for different gap configurations and voltage waveshapes.

Fig. 22 shows a comparison between experimental [11] and computed results.

Overall model results are in good agreement with experimental observation even if, in the case of short times to crest, the model seems to underestimate the time to breakdown. Further experimental data would be needed to test the validity of some input parameters like the R_C line capacitance (used in the simulation of the relaxation process), or the stem geometric parameters (used to determine the threshold for pilot inception).

5. Conclusions

The presented investigation and results have shown that the actual understanding of the physical mechanism of electrical discharge is good enough for the development of self consistent detailed models, ranging from short gap streamer breakdown to long gaps or atmospheric discharge; these models can give account of the breakdown field variations with gap length on the basis of the internal fields of the different phases of the discharge. In particular the transition to 'thermalized leader' can explain the capability of natural lightning to propagate in external fields as low as few hundreds of $V \cdot m^{-1}$.

References

[1] J. Willett, D.A. Davis, P. Laroche, An experimental study of positive leaders initiating rocket-triggered lightning, Atmosph. Res. 51 (1999) 189–219.

[2] V. Idone, The luminous development of Florida triggered lightning, Res. Lett. Atmos. Electr. 12 (1992) 23–28.

[3] P. Laroche, V. Idone, A. Eybert-Berard, L. Barret, Observations of bi-directional leader development in a triggered lightning flash, International Aerospace and Ground Conference on Lightning and Static Electricity (ICOLSE), NASA, Coco Beach, Floride, 1991.
[4] M.A. Uman, E.P. Krider, A review of natural lightning: experimental data and modelling, IEEE Trans. Electromag. Comp. EMC 24 (1982) 79–112.
[5] A. Bondiou-Clergerie, P. Lalande, P. Laroche, P. Willet, J.C. Davis, I. Gallimberti, The inception phase of positive leaders in triggered lightning: comparison of modeling with experimental data, 11th International Conference on Atmospheric Electricity, Huntsville (USA), 1999.
[6] A. Bondiou, I. Gallimberti, Theoretical modelling of the development of the positive spark in long gaps, J. Phys. D 27 (1994) 1252–1266.
[7] G. Bacchiega, A. Gazzani, M. Bernardi, I. Gallimberti, A. Bondiou-Clergerie, Theoretical modelling of the laboratory negative stepped-leader, ICOLSE, Mannheim, Germany, 1994.
[8] A. Castellani, A. Bondiou-Clergerie, P. Lalande, A. Bonamy, I. Gallimberti, Laboratory study of the bi-leader process from an electrically floating conductor, IEE Proc.: Sci. Measurement and Technology 145 (5) (1998) 193–199.
[9] P. Lalande, A. Bondiou-Clergerie, G.L. Bacchiega, I. Gallimberti, Observation and modeling of lightning leaders, C. R. Physique 3 (2002) 1375–1392.
[10] Les Renardières Group, Positive discharges in long air gaps at Les Renardières – 1975 results and conclusions, Electra 53 (1977).
[11] Les Renardières Group, Negative discharges in long air gaps at Les Renardières – 1978 results, Electra 74 (1981).
[12] H. Raether, Electron Avalanches and Breakdown in Gases, Butterworths, London, 1964.
[13] I. Gallimberti, A computer model for streamer propagation, J. Phys. D 5 (1972) 2179–2189.
[14] L. Loeb, J.M. Meek, The mechanism of the electric spark, Stanford University Press, Stanford, CA, 1941.
[15] F.W. Peek, Dielectric Phenomena in High Voltage Engineering, McGraw-Hill, 1929.
[16] G. Hartmann, Spectroscopie de la décharge couronne, PR D Thesis, Paris, 1977.
[17] E. Marode, The mechanism of spark breakdown in air at atmospheric pressare between a positive pint and a plane, J. Appl. Phys. 46 (1975) 2005–2020.
[18] I. Gallimberti, The mechanism of long spark formation, J. Phys. Coll. C7 40 (7) (1979) 193–250.
[19] S. Badaloni, I. Gallimberti, E. Marode, A simplified model of streamer formation in weakly electronegative gases, non publié, 1992.
[20] C.T. Phelps, Field enhanced propagation of corona streamers, J. Geophys. Res. 76 (1971) 5799–5806.
[21] N. Goelian, P. Lalande, A. Bondiou-Clergerie, G. Bacchiega, A. Gazzani, I. Gallimberti, A simplified model for the simulation of the positive spark development in long air gaps, J. Phys. D 30 (17) (1997) 2441–2452.
[22] Les Renardières Group, Research on long air gap discharges at Les Renardières, Electra 23 (1972).
[23] Les Renardières Group, Long air gap discharges at Les Renardières : 1973 results, Electra 35 (1974).
[24] S.I. Braginskii, Theory of the development of the spark channel, Soviet Phys. JETP 34 (1958) 1068–1074.
[25] M.M. Kekez, P. Savic, An hypersonic interpretation of the development of the spark channel in gases, J. Phys. D 7 (1974) 620–628.
[26] M.M. Kekez, P. Savic, Further support for the hypersonic and Volterra models of spark channel development, IEE 4th Int. Conf. Gas Discharges, Swansea, 1976.
[27] M.T. Leu, Biondi, A. Manfred, R. Johnesen, Measurement of the recombination of electrons with $H_3O^+(H_2O)_n$ series ions, Phys. Rev. A 7 (1973) 292.
[28] R.T. Waters, Leader and space charge characteristics derived from fluxmeter results, Electra 35 (1974) 110–116.
[29] R.T. Waters, Space charge and energy storage in spere plane gaps, Electra 53 (1977) 77–85.
[30] R. Brambilla, A numerical model for the radial expansion of high current leader channel, 5th Int. Conference on Gas Discharges, Liverpool, 1978.
[31] I. Gallimberti, The characteristics of the leader channel in long air gaps, World Electrotech. Conf., Moscow, 1977.
[32] A. Castellani, Calcul du champ électrique par la méthode des charges équivalentes pour la simulation d'une décharge bi-leader, Thèse de doctorat de l'Université Paris XI, 1995.
[33] P. Ortega, P. Domens, A. Gibert, B. Hutzler, G. Riquel, Performance of a 16.7 m air rod-plane gap under a negative switching impulse, J. Phys. D 27 (1994) 2379–2387.